Atmospheric
Chemistry
and Physics

Detailed budget analysis of HONO in central London reveals a missing daytime source

J. D. Lee[1,2]**, L. K. Whalley**[3,4]**, D. E. Heard**[3,4]**, D. Stone**[4]**, R. E. Dunmore**[2]**, J. F. Hamilton**[2]**, D. E. Young**[5,a]**, J. D. Allan**[5,6]**,
S. Laufs**[7]**, and J. Kleffmann**[7]

[1]National Centre for Atmospheric Science, University of York, York, UK
[2]Department of Chemistry, University of York, York, UK
[3]National Centre for Atmospheric Science, University of Leeds, Leeds, UK
[4]School of Chemistry, University of Leeds, Leeds, UK
[5]School of Earth, Atmospheric and Environmental Sciences, University of Manchester, Oxford Road,
Manchester, M13 9PL, UK
[6]National Centre for Atmospheric Science, University of Manchester, Oxford Road, Manchester, M13 9PL, UK
[7]Physikalische und Theoretische Chemie/Fakultät Mathematik und Naturwissenschaften,
Bergische Universität Wuppertal (BUW), Gaußstr. 20, 42119 Wuppertal, Germany
[a]now at: Department of Environmental Toxicology, University of California, Davis, CA 95616, USA

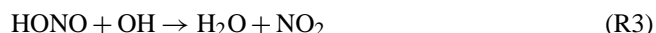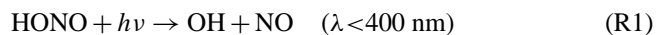*Correspondence to:* J. D. Lee (james.lee@york.ac.uk)

Abstract. Measurements of HONO were carried out at an urban background site near central London as part of the Clean air for London (ClearfLo) project in summer 2012. Data were collected from 22 July to 18 August 2014, with peak values of up to 1.8 ppbV at night and non-zero values of between 0.2 and 0.6 ppbV seen during the day. A wide range of other gas phase, aerosol, radiation, and meteorological measurements were made concurrently at the same site, allowing a detailed analysis of the chemistry to be carried out. The peak HONO / NO_x ratio of 0.04 is seen at $\sim$ 02:00 UTC, with the presence of a second, daytime, peak in HONO / NO_x of similar magnitude to the night-time peak, suggesting a significant secondary daytime HONO source. A photostationary state calculation of HONO involving formation from the reaction of OH and NO and loss from photolysis, reaction with OH, and dry deposition shows a significant underestimation during the day, with calculated values being close to 0, compared to the measurement average of 0.4 ppbV at midday. The addition of further HONO sources from the literature, including dark conversion of NO_2 on surfaces, direct emission, photolysis of ortho-substituted nitrophenols, the postulated formation from the reaction of $HO_2 \times H_2O$ with NO_2, photolysis of adsorbed HNO_3 on ground and aerosols, and HONO produced by photosensitized conversion of NO_2 on the surface increases the daytime modelled HONO to 0.1 ppbV, still leaving a significant missing daytime source. The missing HONO is plotted against a series of parameters including NO_2 and OH reactivity (used as a proxy for organic material), with little correlation seen. Much better correlation is observed with the product of these species with $j(NO_2)$, in particular NO_2 and the product of NO_2 with OH reactivity. This suggests the missing HONO source is in some way related to NO_2 and also requires sunlight. Increasing the photosensitized surface conversion rate of NO_2 by a factor of 10 to a mean daytime first-order loss of $\sim$ 6 $\times 10^{-5}$ s^{-1} (but which varies as a function of $j(NO_2)$) closes the daytime HONO budget at all times (apart from the late afternoon), suggesting that urban surfaces may enhance this photosensitized source. The effect of the missing HONO to OH radical production is also investigated and it is shown that the model needs to be constrained to measured HONO in order to accurately reproduce the OH radical measurements.

1 Introduction

The hydroxyl radical (OH) is the main daytime oxidant in the troposphere, playing a key role in the chemical transformations of trace species (Levy, 1971). A major source of OH, especially in polluted environments, is the photolysis of nitrous acid (HONO) in the near UV region (Reaction R2). It has been shown in numerous studies that HONO can actually be the dominant early morning source of OH (Ren et al., 2003, 2006; Dusanter et al., 2009; Michoud et al., 2012) and has often been shown to also be significant during the rest of the day (Elshorbany et al., 2009; Hofzumahaus et al., 2009; Villena et al., 2011; Michoud et al., 2014). This is mainly due to unexpectedly high levels of HONO measured during daylight hours when fast photolysis would have been expected to keep concentrations low and hence insignificant for a source of OH. As a result of these studies, it has become clear that HONO has the ability to initiate and accelerate daytime photochemistry and hence knowledge of its formation and loss are crucial to understanding tropospheric oxidation chemistry.

Typically, HONO in the troposphere would be expected to be governed by formation by the reaction between nitric oxide (NO) and OH (Reaction R2) and losses by photolysis (Reaction R1) and oxidation by OH (Reaction R3).

$$HONO + h\nu \rightarrow OH + NO \quad (\lambda < 400\text{ nm}) \tag{R1}$$

$$OH + NO + M \rightarrow HONO + M \tag{R2}$$

$$HONO + OH \rightarrow H_2O + NO_2 \tag{R3}$$

These reactions can be used, along with measurements of concentrations of the relevant species and HONO photolysis rates, to calculate a photochemical steady state concentration of HONO. Such calculations from field studies typically show a peak of HONO at night (when there is no photolysis), with levels in the low pptv range during the day. However, measurements usually show that daytime HONO levels can reach substantially higher concentrations than this, with mixing ratios up to a few hundred pptv frequently observed (Zhou et al., 2002; Kleffmann et al., 2005; Acker et al., 2006). It is clear from these analyses that there is an extra source of HONO present, which can have a significant impact on the atmospheric oxidising capacity due to its potential to form OH. A range of reactions have been postulated during the various studies to account for the missing source of HONO, with these likely to be heterogeneous either on aerosols or the ground itself. Major ground surfaces were recently confirmed by direct flux measurements of HONO (Ren et al., 2011; Zhou et al., 2011; Zhang et al., 2012). Tower measurements (Harrison and Kitto, 1994; Kleffmann et al., 2003; Oswald et al., 2015; Sörgel et al., 2011a, 2015; Stutz et al., 2002; Vandenboer et al., 2013; Villena et al., 2011; Vogel et al., 2003; Wong et al., 2012; Young et al., 2012) and aircraft observations (Li et al., 2014; Zhang et al., 2009) have also demonstrated that major HONO sources exist at canopy or ground surfaces through the measurement of vertical gradients. It is postulated that such processes involve the conversion of nitrogen dioxide (NO$_2$) or nitric acid (HNO$_3$) to HONO on ground surfaces and are enhanced by sunlight, thus providing a daytime-only source of HONO (Zhou et al., 2003; George et al., 2005). In addition, bacterial production of nitrite in soil surfaces were also proposed as additional HONO source (Su et al., 2011, Oswald et al., 2013). It has also been shown that HONO is emitted directly from petrol and diesel vehicle exhausts (Kurtenbach et al., 2001; Li et al., 2008). At most sites, this is a relatively small contributor to HONO due to its relatively short atmospheric lifetime in the daytime (10–20 min); however close to major roads and especially in tunnels it can contribute greatly to the HONO present. A recent publication by Michoud et al. (2014) gives a good summary of the possible daytime HONO sources under similar conditions to this study (in Paris) and a review by Kleffmann (2007) also discusses daytime HONO sources in depth.

Almost all previous field studies still show a significant missing daytime HONO source, thus showing the requirement for more studies. In this work we report what are, to our knowledge, the first measurements of HONO made in London, UK, one of the largest cities in Europe. The measurements were made as part of the summer intensive operation period (IOP) of the Clean Air for London (ClearfLo) project and, as a result, were made concurrently with a wide range of other atmospheric gas and aerosol phase species (including OH, HO$_2$, NO, NO$_2$, and photolysis rates). This has enabled us to undertake a detailed modelling study of HONO using the Master Chemical Mechanism (MCMv3.2), in which we included a series of known sources of HONO found in the literature. We then investigate the difference between daytime measured and modelled HONO, with a simple correlation analysis against other measured parameters. The model was also used to assess the radical forming potential of the missing HONO, which can ultimately lead to increased production of secondary pollutants such as ozone (O$_3$) and secondary organic aerosol (SOA).

2 Experimental

The ClearfLo project had the aim of providing an integrated measurement and modelling program in order to help better understand the atmospheric processes that affect air quality (Bohnenstengel et al., 2014). As part of ClearfLo, a summer IOP took place in July and August 2012 that involved the measurement of a wide range of gas and aerosol phase species (including meteorology), which enabled a detailed study of the atmospheric chemistry of London's air to be carried out.

2.1 Site description

The main site for the IOP was an urban background site at the Sion Manning School in North Kensington, London ($51°31'16''$ N, $0°12'48''$ W), which is situated in a residential area approximately 7 km west of central London (defined here as Oxford Street). Measurements of NO, NO_2 and total reactive nitrogen (NO_y), sulphur dioxide (SO_2), O_3, carbon monoxide (CO), PM_{10}, and total particle number concentration have been routinely made at the site since January 1996 as part of the Automatic Urban and Rural Network (AURN) and the London Air Quality Network (LAQN) (Bigi and Harrison, 2010). For the ClearfLo IOP, other instruments were installed in various shipping container laboratories in the grounds of the school, all within 20 m of the long-term measurements. A full description of the campaign, including the instruments present can be found in Bohnenstengel et al. (2014), and details of the measurements pertinent to this work are given below. All measurements were carried out at a height of around 5 m above ground level, within a horizontal area of 10 m from each other.

2.2 HONO measurements

HONO was measured using a long-path absorption photometer (LOPAP) instrument from the University of Wuppertal, Germany, which is explained in detail elsewhere (Heland et al., 2001). Briefly, gaseous HONO is sampled in a stripping coil containing a mixture of sulfanilamide in a 1M HCl solution and is derivatized into an azo dye. The light absorption by the azo dye is measured in a long-path absorption tube by a spectrometer at 550 nm using an optical path length of 2.4 m. The stripping coil was placed directly in the atmosphere being sampled; this means that the length of the glass inlet was only 2 cm, minimizing sampling artefacts. The LOPAP has two stripping coils connected in series to correct interferences. In the first coil (channel 1), HONO is trapped quantitatively together with a small amount of the interfering substances. Assuming that these interfering species are trapped in a similar amount in the second coil (channel 2), the difference between the signals of the two channels provides an interference-free HONO signal. Zero measurements were performed every 7 h. Calibrations of the spectrometer using a known concentration of the derivatized azo dye were carried out three times during the campaign. The instrument was previously successfully validated against the spectroscopic differential optical absorption spectroscopy (DOAS) technique under urban conditions and in a smog chamber (Kleffmann et al., 2006). During the campaign a detection limit of 1 pptV (for a time resolution of 5 min), a precision of 1 % and an accuracy of 10 % were obtained.

2.3 Radical measurements

OH, HO_2, and RO_2 radical concentrations were measured using the FAGE (fluorescence assay by gas expansion) technique (Heard and Pilling, 2003). In the case of HO_2 and RO_2, the radicals were first titrated with NO to OH before FAGE detection. The current mode of operation is described in detail elsewhere (Whalley et al., 2015). The HO_2 observations used as a constraint in the modelling studies reported in Sect. 3.3 were made using a low flow of NO (7.5 sccm), which laboratory tests have shown minimized interferences from alkene and aromatic-derived RO_2 species (Whalley et al., 2013). Under this regime, the interference from RO_2 radicals present is estimated to contribute < 3 % to the HO_2 concentration. The limit of detection at a signal-to-noise ratio of 3 for one data acquisition cycle was $\sim 1.3 \times 10^6$ molecule cm^{-3} for OH and $\sim 6.3 \times 10^6$ molecule cm^{-3} for HO_2. The measurements were recorded with 1 s time resolution, and the accuracy of the measurements was ~ 15 %.

2.4 Other supporting measurements

The NO and NO_2 data used in this work were taken using an Air Quality Design Inc. custom-built high-sensitivity chemiluminescence analyser with LED based blue light NO_2 converter. The instrument consists of two channels measuring NO by reaction with excess O_3 to form excited state NO_2 followed by the detection of the resultant chemiluminescence (Drummond et al., 1985; Lee et al., 2009). The air flow in one of the channels first passes through a photolytic converter where light at 395 nm from an array of LEDs photolyses NO_2 to NO. The 395 nm wavelength has a specific affinity for NO_2 photolytic conversion to NO, giving high analyte selectivity within the channel, and there is a low probability of other species (such as HONO) being photolysed (Pollack et al., 2010). This makes this measurement a significant improvement over the high-temperature catalytic NO_2 conversion used for the long-term measurement at the North Kensington site (Steinbacher et al., 2007; Villena et al., 2012). Calibration of the instrument was carried out every 2 days using 5 ppm NO in nitrogen (BOC – certified to the UK National Physical Laboratory (NPL) scale) – diluted to ~ 20 ppb using high-purity zero air (BOC BTCA 178). The NO_2 conversion efficiency (ca. 40 %) was calibrated using gas phase titration of the NO standard by O_3. NO_y data were taken using a TEI 42i TL NO analyser with Molybdenum converter.

Volatile organic compound (VOC) measurements were obtained using two gas chromatography (GC) instruments. The volatile fraction of VOCs (C_2-C_7 hydrocarbons, with a small selection of oxygenated VOCs, or OVOCs) was measured using a dual channel GC-FID (flame ionization detector) (Hopkins et al., 2003), while a comprehensive two dimensional GC (GC $\times$ GC-FID) measured the less volatile fraction (C_6-C_{13}, with a large group of OVOCs) (Lidster et al., 2014).

Measurements of HCHO were made using an Aero-laser 4021 analyser (Salmon et al., 2008). Briefly, gaseous formaldehyde is scrubbed into the liquid phase via a stripping coil containing dilute sulphuric acid. This is followed by reaction with Hantzsch reagent, a dilute solution made with acetyl acetone, acetic acid, and ammonium acetate. Aqueous phase formaldehyde reacts with this reagent via the "Hantzsch reaction" to produce 3,5-diacetyl-1,4-dihydrolutidine (DDL). Once excited by an appropriate wavelength (400 nm in this case) DDL fluoresces, thus allowing quantitative assay by monitoring the emitted light.

Non-refractory $PM_{1.0}$ nitrate, sulphate, organic matter, chloride, and ammonium were quantified using a compact time-of-flight aerosol mass spectrometer (cToF-AMS – Aerodyne Inc.), which gave data with a time resolution of 5 min (Young et al., 2015). Ammonium is reflective of the overall ammonium nitrate because ammonium nitrate is both non-refractory and tends to be in the submicron fraction. While there is supermicron nitrate, it is overwhelmingly in the form of sodium nitrate, which is refractory and not measured by the AMS. It is specifically the nitrate measurement that is of interest here because it pertains to the working hypothesis.

Total aerosol surface area (SA) was calculated using data from an aerodynamic particle sizer instrument (TSI Inc, model 3321). The mean diameter of particles in each size bin (assume spherical) multiplied number of particles in that bin. In total there were 53 size bins ranging from 0.53 to 21.29 μm. Actinic fluxes of solar radiation were measured using a spectral radiometer, which consisted of an Ocean Optics high-resolution spectrometer (QE65000) coupled via fibre optic to a 2π quartz collection dome. These measurements were then used to calculate the photolysis frequencies of a number of > 50 trace gases, including NO_2, HONO, and O_3 ($j(O^1D)$) (Kraus and Hofzumahaus, 1998; Edwards and Monks, 2003). Wind speed and direction, temperature, and relatively humidity were measured using a Davis Vantage Vue met station. Mixing height estimation was based on the vertical profiles of the hourly vertical velocity variance (Barlow et al., 2011). The vertical velocity variance was measured with a Doppler lidar (Halo-Photonics scanning Doppler lidar) located at the North Kensington site with a gate resolution of 18 m; the un-sampled portion of the vertical velocity variance is calculated with the spectral correction technique described in Barlow et al. (2015). The mixing height is defined as the height up to which the vertical velocity variance is higher than $0.1 \, m^2 \, s^{-2}$. This threshold value was perturbed by 20 % (i.e. between 0.08 and $0.121 \, m^2 \, s^{-2}$) and the median of the estimated values was taken as the hourly mixing height.

3 Results

3.1 Overview of data

Data were collected from 22 July to 18 August 2012 and time series of local wind speed, wind direction, NO, NO_2, O_3, HONO, and the photolysis rate of HONO ($j(HONO)$) are shown in Fig. 1. The majority of the measurement period was characterized by south-westerly winds, with the wind speed showing a diurnal cycle of less than $1 \, m \, s^{-1}$ at night (the minimum measurable by the anemometer) to 4–$6 \, m \, s^{-1}$ in late afternoon. These periods show NO and NO_2 with peaks of 15 and 10 ppbV respectively, typically at $\sim$ 07:30 UTC, the peak of the morning rush hour. O_3 shows a diurnal cycle with a typical maximum of 40–45 ppbV at $\sim$ 16:00 UTC and minima of < 20 ppbV at night. The exceptions to this are two periods from 24 to 27 July and 8 to 10 August, during which the site was subjected to generally easterly flow, with lower wind speed. Due to central London being to the east of the site, these periods are characterized by higher levels of NO_x (up to 60 ppbV of NO and 50 ppbV of NO_2), which has its source mainly from traffic exhaust. O_3 is also higher during these periods due to a combination of the higher primary pollution levels (NO_x and VOCs) and low wind speeds causing a build-up of this secondary pollutant during the 3- to 4-day period. Peak daytime levels of O_3 of 60–100 ppbV are observed during these more polluted periods. HONO concentrations show peak values at night throughout the campaign (up to 1.8 ppbV during the easterly periods and up to 0.7 ppbV during the rest of the campaign), with non-zero values seen during the day (0.3–0.6 ppbV).

This behaviour is better visualized using the average diurnal cycle, which is shown for HONO and NO_x in Fig. 2a and $j(HONO)$ and the HONO / NO_x ratio in Fig. 2b. In addition to the total campaign average, diurnal cycles are shown for the easterly and westerly time periods described above. NO_x follows an expected profile, with a peak of 29 ppbV on average during the morning rush hour at $\sim$ 05:30 UTC (06:30 local time), followed by a decrease during the day, due largely to increasing boundary layer (BL) depth and hence dilution. After $\sim$ 16:00 UTC, the NO_x levels begin to rise from a minimum of 8.5 ppbV due to a combination of increased emissions during the evening rush hour and the reduction of the BL depth into the night. Concentrations reach $\sim$ 18 ppbV by midnight and remain reasonably constant throughout the rest of the night. Diurnal averages in the easterly and westerly conditions follow the same pattern as for the total data series, with significantly higher NO_x during the easterly period. During the morning peak, NO_x is a factor of 3 higher during easterly flow compared to westerly and 15–20 % higher during the daytime. HONO appears to follow a similar diurnal profile to NO_x, which is not unexpected since the main known HONO sources involve nitrogen oxides. However, the morning peak of HONO is around 1 h earlier compared to NO_x (at around 04:30 UTC) due to
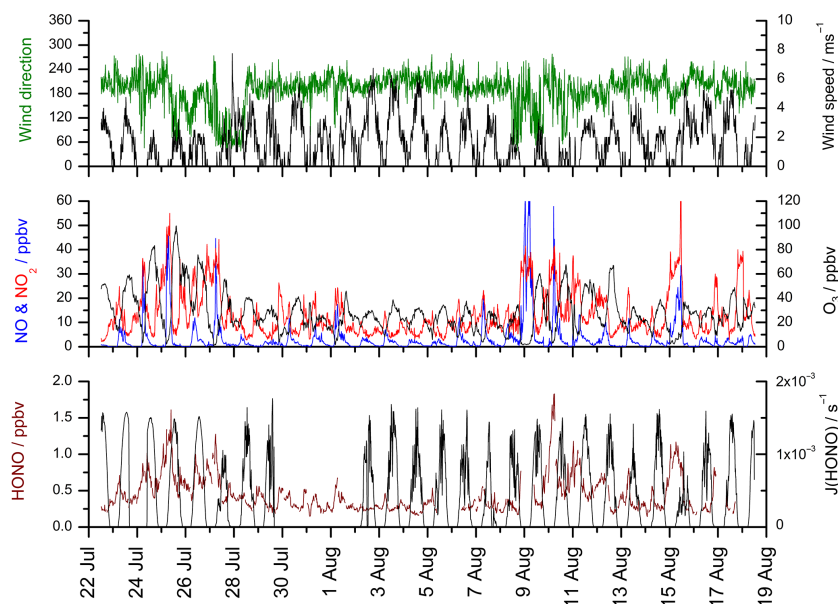
Figure 1. Time series of selected data from the ClearfLo intensive operation period (July and August 2012). The top panel shows wind speed (black) and wind direction (green); the middle panel shows NO (blue), NO_2 (red), and O_3 (black); the bottom panel shows HONO (dark red) and j(HONO) (black). All data are 15 minute averaged and plotted as UTC (local time − 1 h).
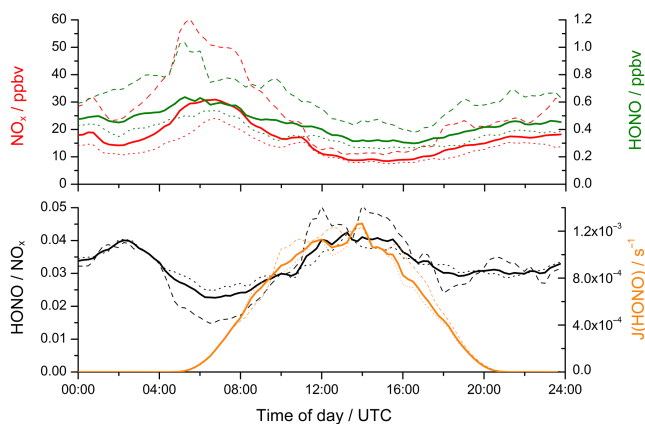

Figure 2. Average diurnal profiles of selected data from the IOP. The top panel shows total NO_x (red) and HONO (green), and the bottom panel shows j(HONO) (orange) and the HONO / NO_x ratio (black). Profiles were generated by binning all data in a 15 min time period together. For each, the solid line is the total of all days, the dashed line is data from easterly conditions, and the dotted line data from westerly conditions (see text for dates).

the onset of HONO photolysis at sunrise. HONO concentrations are also higher under easterly flow conditions compared to westerly, with the early morning peak being a factor of around 2 higher and the daytime average around 25 % higher. The behaviour of HONO is perhaps better described by looking at the HONO / NO_x ratio and the average diurnal cycle of HONO / NO_x and j(HONO) is shown in Fig. 2b. The peak HONO / NO_x of 0.04 is seen at ∼ 02:00 UTC due

to the lack of photolysis (the major loss route for HONO), direct HONO emissions, and heterogeneous HONO formation at the surface during the night into a relatively shallow BL. After this (and before sunrise), the ratio begins to decrease due to the onset of fresh NO_x emissions and continues to decrease during the morning due to the increase of HONO photolysis. If the HONO sources which are active during night-time are the only active sources also during daytime, the HONO / NO_x ratio should show a deep minimum around noon. In contrast, in Fig. 2 a maximum is observed, which is a hint to an additional daytime source. In addition, the maximum of HONO / NO_x correlates well with the radiation, which is again a hint of a photochemical process.

The HONO levels measured in London are within the range of data published from other urban sites, although there is a wide range of concentrations reported in the literature. Michoud et al. (2014) reported daytime levels of 0.11 ppbV (averaged for 3 h around local solar noon) at a site near Paris, France, which is lower than our value of 0.44 ppbV. However, the site was 14 km from the centre of Paris (upwind), significantly further away from the major emission sources than the London site. As a result, NO_x was lower in Paris, with a daytime campaign average of 5.3 ppbV compared to our value of 13.9 ppbV, giving a daytime HONO / NO_x ratio of 0.020 compared to our value of 0.031, although this may be partially explained by the lower j(HONO) values in London compared to Paris. The fact that the London site is closer to emission sources will most likely also influence this, as direct emission of HONO from traffic exhaust is potentially a significant proportion of HONO in large cities (Kurten-

bach et al., 2001). Kleffmann et al. (2006) reported daytime HONO levels of between 0.2 and 0.3 ppbv in Milan, Italy. They also compared data from a LOPAP instrument (similar to that used in this study) and a DOAS instrument and showed excellent agreement. The resultant HONO / NO$_x$ ratio reported was 0.046. Wong et al. (2012) reported daytime HONO mixing ratios averting 0.1 ppbv in Houston, USA, with corresponding average daytime NO$_x$ of 10 ppbv, giving a HONO / NO$_x$ ratio of 0.03. Some other studies in large cities have reported larger daytime HONO concentrations, e.g. Santiago, Chile (1.5 ppbV) (Elshorbany et al., 2009), Guangzhou, China (2.0 ppbV) (Qin et al., 2009), and Xinken, China (0.80 ppbV) (Su et al., 2008a, b); however, all of these were at sites with much larger NO$_x$ loading and so the resultant HONO / NO$_x$ ratio is similar to the measurements in London. The range of ambient HONO values reported in the literature suggest that the specific conditions at a particular site are key to the HONO levels, in particular the prevalence of different levels of NO$_x$ during daylight hours. Thus a modelling study including a range of known HONO sources and sinks is required to fully understand the observed behaviour.

3.2 HONO photostationary state approach

In order to initially assess HONO concentrations and in particular the impact of any potential extra sources during this campaign, a photostationary state (PSS) calculation has been carried out. In this approach, the sources and sinks of the species in question are assumed to balance each other and is thus only suitable for species with a short lifetime, such as free radicals. However, it has been widely used to study the daytime HONO budget, despite its lifetime being in the range of 10–20 min during the day (Alicke et al., 2002; Wong et al., 2012), resulting in significant uncertainties, especially for measurements close to emission sources (Lee et al., 2013). However, the measurement site in this study is described as an urban background site and thus is relatively free from the influence of major roads or point sources. Calculation of the transport time since emission using the NO$_x$ / NO$_y$ ratio (using the technique described in Cappa et al., 2012) shows a lifetime since emission of 40–50 min, significantly greater than the photochemical lifetime of HONO (typically 10–20 min at noon). Thus, we still consider the PSS approach a useful tool to quantify HONO sources during daytime. HONO is expected to be in photostationary state due to its formation by the reaction between OH and NO, its sinks by rapid photolysis (to reform OH and NO), its reaction with OH, and its dry deposition. Combining these terms, the concentration [HONO]$_{PSS}$ can be calculated using the following Eq. (1):

$$\text{HONO}_{\text{PSS}} = \frac{k_{\text{OH+NO}}[\text{OH}][\text{NO}]}{k_{\text{OH+HONO}}[\text{OH}] + j(\text{HONO}) + \frac{\nu_{\text{HONO}}}{h}}. \qquad (1)$$

Measured data were used for OH, NO, and j(HONO), with the relevant pressure and temperature-dependant rate constants for $k_{\text{OH+NO}}$ and $k_{\text{OH+HONO}}$ taken from Atkinson et al. (2004). ν_{HONO} is the deposition velocity of HONO, set at an upper limit of $3.0 \, \text{cm s}^{-1}$, and h is the BL height. We use an effective HONO BL height of 75 m, calculated using typical Eddy diffusion coefficients and j(HONO), as the likely height to which HONO will reach, given a daytime lifetime of 15 min. This method will strongly underestimate HONO deposition because the BL height will be considerably larger than the height at which HONO will actually be transported to due to its short lifetime (10–20 min during the day). This effect is partly compensated for by using $3.0 \, \text{cm s}^{-1}$ for the deposition velocity, which is at the upper end of the ranges quoted in the literature (Harrison and Kitto, 1994; Stutz et al., 2002; Trebs et al., 2006); however it does mean there are considerable errors in this approach. The PSS analysis also does not consider vertical structure, thus the magnitude of any unknown source inferred from the analysis will be dependent on the height above the ground surface that the measurements are being made. The average daytime diurnal profiles in both easterly and westerly conditions are shown in Fig. 3. We do not consider night-time data as the PSS approach would not be valid at night. We only consider data from 08:00 UTC (j(HONO) $> 4 \times 10^{-4} \, \text{s}^{-1}$), a time at which all HONO produced during the night will have been lost due to photolysis after sunrise. It is clear that the PSS calculation cannot replicate the measured HONO during daylight hours (08:00–20:00 UTC). The PSS does appear to reproduce the daylight cycle of HONO, with high concentrations during the morning peak between 06:00 and 09:00 UTC due to the increase in NO and OH at the morning rush hour. However, after this morning peak, HONO$_{\text{PSS}}$ rapidly decreases to < 0.05 ppbV by midday, followed by a gradual decrease during the afternoon reaching a minimum of 0.007 ppbv at 19:30 UTC. This is due to the rapid photolysis of HONO, which occurs in the near-UV region and occurs significantly faster than the only production route in the PSS calculation (OH + NO), especially during the later part of the day when NO is low. HONO$_{\text{PSS}}$ during the day shows similar levels in both easterly and westerly conditions, despite measured HONO being significantly higher in the more polluted easterly regime. The PSS treatment of HONO is clearly incomplete, with significant missing source terms.

3.3 HONO box model approach

In order to assess the importance of other potential HONO sources in our study, we use a photochemical model based on the Master Chemical Mechanism (MCMv3.2) (Jenkin et al., 2012). Complete details of the kinetic and photochemical data used in the mechanism are available at the MCM website (http://mcm.leeds.ac.uk/MCM/). The model was run with a subset of the MCM and treated the degradation of simultaneously measured trace VOCs, CH$_4$, and CO following oxidation by OH, O$_3$ and NO$_3$ and included $\sim 15\,000$ reactions and ~ 3800 species. The model was constrained to measurements
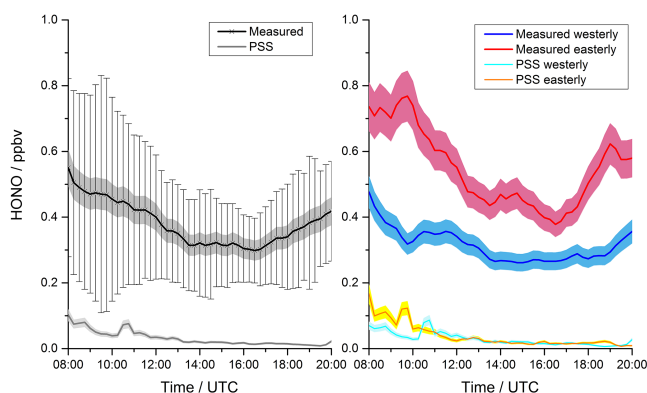
Figure 3. Averaged diurnal profiles (daylight hours) of measured (black) and photostationary state (PSS) calculated (grey) HONO (left panel). The shaded area represents instrumental ($\pm 10\%$) and model ($\pm 17\%$) error; the bars represent the standard deviation of the measurements. The right panel shows averaged diurnal profiles of measured and PSS HONO divided into easterly (red/orange) and westerly (blue/cyan) conditions. The shaded area represents the measurement ($\pm 10\%$) and PSS ($\pm 17\%$) error.
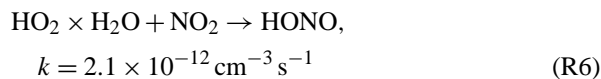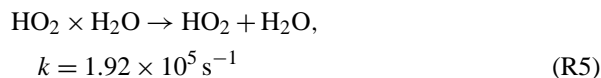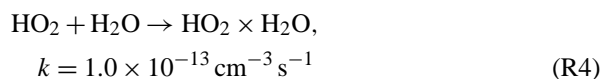
of NO, NO_2, O_3, CO, CH_4, 62 individual VOC species measured by GC-FID, as well as 2D-GC, PAN, HCHO, HNO_3, HO_2, water vapour, temperature, and pressure. The model was constrained with the measured photolysis rates (including $j(O^1D)$, $j(NO_2)$, $j(HONO)$, $j(HCHO)$, $j(CH_3COCH_3)$, and $j(CH_3CHO)$). A constant H_2 concentration of 500 ppbV was assumed (Forster et al., 2012). The model inputs were updated every 15 min. For species measured more frequently, data were averaged to 15 min intervals, whilst those measured at a lower time resolution were interpolated. The loss of all non-constrained model-generated species by a wind-speed-dependent deposition (ν) was calculated by summing the resistances $1/R_a$, $1/R_b$, and $1/R_c$, for which R_a describes turbulent convective transport, R_b the laminar diffusion near the surface, and R_c the surface resistance. The inverse of the surface resistances ($1/R_c$) assumed are $3\,\text{cm}\,\text{s}^{-1}$ for HNO_3 and $2\,\text{cm}\,\text{s}^{-1}$ for HONO and $1\,\text{cm}\,\text{s}^{-1}$ for NO_2 (and all other non-constrained model species). For the campaign, average wind speed of $1.6\,\text{m}\,\text{s}^{-1}$, ν_{HNO_3}, ν_{HONO}, and ν_{NO_2} equals 0.52, 0.48, and $0.38\,\text{cm}\,\text{s}^{-1}$ respectively. As with the steady state approach, we use an effective HONO BL height of 75 m in the model. This assumption leads to a campaign average first-order loss of HONO (at a mean wind speed of $1.6\,\text{m}\,\text{s}^{-1}$) of $\nu_{HONO}/\text{BL} = 6.4 \times 10^{-5}\,\text{s}^{-1}$. The model was run for the entirety of the campaign in overlapping 7-day segments. To allow all the unmeasured model-generated intermediate species time to reach steady state concentrations, the model was initialized with inputs from the first measurement day (22 July) for 5 days before comparison to measurements were made. Comparison of these 5 spin-up days demonstrated that the concentration of model-generated species rapidly converged and there was less than a 1 % dif-

ference in (for example) modelled OH or HONO concentration by the second spin-up day. As a result of this, the model segments were run so as to overlap for 2 days only to reduce the computing time. The model was run unconstrained to HONO (for the results presented in this paper) for comparison with measured HONO concentration.

A number of HONO sources in addition to the gas phase source from the reaction of hydroxyl radicals with NO have been included in the model. These include the following.

a. A direct emission source of HONO was added to the model, using a ratio of HONO / NO_x of 0.008 reported previously from tailpipe emission studies of NO_x and HONO in a tunnel (Kurtenbach et al., 2001) and the measured NO_x concentrations. It is likely that the used value represents an upper limit of the direct emission contribution to HONO during daytime due to the short atmospheric lifetime of HONO (10–20 min) compared to NO_x.

b. It has been suggested that a reaction between $HO_2 \times H_2O$ and NO_2 could produce HONO at a sufficiently fast rate to be a significant source in the troposphere (Li et al., 2014). It had previously been shown in laboratory studies that this reaction produces negligible HONO yields under dry conditions (Tyndall et al., 1995; Dransfield et al., 2001). However, in the lower troposphere, around 30 % of HO_2 is suggested to be present as an $HO_2 \times H_2O$ complex and hence may show different chemical behaviour. Kinetic measurements of the self reaction $HO_2 + HO_2$ have revealed the chaperone effect of water vapour enhancing the rate coefficient (Stone and Rowley, 2005). It has also been shown that the rate coefficient of the reaction $HO_2 + NO_2$ increase by 50 % from dry to humid atmospheric conditions (Sander and Peterson, 1984). In the Li et al. (2014) study it was postulated that the reaction converts NO_2 to HONO with a yield of 100 % and this allowed a model to reproduce the observed levels of HONO, albeit under free-tropospheric conditions away from surfaces. Inclusion of this reaction also improved the agreement between the model and measured levels of HO_2 and NO_x. However, recent field data have shown that in fact this reaction produces only a 3 % yield of HONO (Ye et al., 2015), thus greatly reducing the impact of the reaction on HONO production. Nevertheless, the following additional reactions were included in our MCM model to account for the equilibrium that exists between uncomplexed and H_2O-complexed HO_2 in the atmosphere (Reactions R4 and R5) and the major reactions of H_2O-complexed HO_2 in this urban environment (Re-

actions R6 and R7).

$$HO_2 + H_2O \rightarrow HO_2 \times H_2O,$$
$$k = 1.0 \times 10^{-13}\,\mathrm{cm}^{-3}\,\mathrm{s}^{-1} \tag{R4}$$

$$HO_2 \times H_2O \rightarrow HO_2 + H_2O,$$
$$k = 1.92 \times 10^{5}\,\mathrm{s}^{-1} \tag{R5}$$

$$HO_2 \times H_2O + NO_2 \rightarrow HONO,$$
$$k = 2.1 \times 10^{-12}\,\mathrm{cm}^{-3}\,\mathrm{s}^{-1} \tag{R6}$$

$$HO_2 \times H_2O + NO \rightarrow OH + NO_2,$$
$$k = 3.60 \times 10^{-12}(e^{(270/T)})\,\mathrm{cm}^{-3}\,\mathrm{s}^{-1} \tag{R7}$$

c. Light-induced heterogeneous conversion of NO_2 to HONO on aerosol surfaces was also considered assuming an uptake coefficient of 10^{-6} (Kleffmann et al., 1999; Arens et al., 2001; Monge et al., 2010).

d. Heterogeneous conversion of NO_2 to HONO on ground surfaces at a rate equal to $\sim 2 \times 10^{-8}\,\mathrm{s}^{-1}$ has been included in the model, which is consistent with laboratory studies that put an upper limit on dark surface source of $< 10^{-7}$, e.g. Stemmler et al. (2007). This was parameterized in the model by taking the wind-speed-dependent ν_{NO_2} and assuming instantaneous mixing of surface-emitted HONO up to a height of 75 m. This leads to a first-order loss of NO_2 to the ground at a rate of $4 \times 10^{-5}\,\mathrm{s}^{-1}$ on average. This rate was scaled down by a factor of 2000 to represent the dark surface conversion of NO_2 to HONO reported in laboratory studies. However, it has to be stressed that the present calculation strongly underestimates the contribution of heterogeneous HONO formation on ground surfaces, especially during night-time at the measurement height, caused by the assumption of an instantaneous mixing up to a height of 75 m; see Eq. (1).

e. A daytime source from the photolysis of ortho-nitrophenols which were not measured during the campaign but have been estimated to be present at an upper limit constant concentration of 1 ppbV and which photolyse at a rate of $\sim 3 \times 10^{-5}\,\mathrm{s}^{-1}$ at midday (Bejan et al., 2006).

f. Photolysis of adsorbed HNO_3 on ground surfaces has been reported to produce HONO (Zhou et al., 2003, 2011). We have estimated the concentration of HNO_3 deposited to the ground surface from the gas phase HNO_3 concentration that was measured during ClearfLo and from the wind-speed-dependent ν_{HNO_3} (Zhou et al., 2011). To assess the maximum impact of this potential HONO source, a noon photolysis rate of surface HNO_3 of $6 \times 10^{-5}\,\mathrm{s}^{-1}$, 2 orders of magnitude faster than $j(HNO_3)_g$ ($j(HNO_3)_{0°SZA} = 6 \times 10^{-7}\,\mathrm{s}^{-1}$) in the gas phase, has been taken (Zhou et al., 2011) and a 100 % HONO yield was assumed.

g. To assess the maximum impact of this potential HONO source, a noon photolysis rate of aerosol NO_3^- of $6 \times 10^{-5}\,\mathrm{s}^{-1}$ and a 100 % HONO yield was again assumed.

h. Photosensitized heterogeneous conversion of NO_2 to HONO on ground surfaces has been parameterized and included in the model by taking a ground surface conversion, which correlates with NO_2 photolysis. A wind-speed-dependent NO_2 deposition velocity calculated using $1/R_c = 1\,\mathrm{cm}\,\mathrm{s}^{-1}$ (Joyce et al., 2014) in 75 m BL leads to a first-order loss of NO_2 to the ground at a rate of $4 \times 10^{-5}\,\mathrm{s}^{-1}$ on average; this is multiplied by a scaling factor equal to $0.25 \times j(NO_2)$, which leads to an overall photosensitized conversion of $NO_2 \rightarrow HONO$ of $\sim 5.6 \times 10^{-6}\,\mathrm{s}^{-1}$ during the day on average. This is consistent with the light-induced conversion of NO_2 to HONO observed in laboratory studies on humic acid surfaces (Stemmler et al., 2007).

We do not include desorption of adsorbed HONO from soil (Oswald et al., 2013, 2015; VandenBoer et al., 2013) as it is still largely speculative, depends on many uncertain variables (soil pH, bacterial activity, soil humidity), and most probably has a very minor contribution under our highly urban conditions (low soil coverage, different expected diurnal contribution).

The full time series of the modelled HONO using the MCM, along with the measured values for the entire measurement campaign, are shown in Fig. 4. Due to the difficulties of predicting night-time chemistry with a photochemical model (such as the MCM), we only consider the daytime here (08:00–20:00 UTC). The time series show that predicted daytime HONO using the full model is higher than from the simple PSS calculation; however, it can be seen that the predicted daytime HONO is still lower than the measurement on all days and falls outside the 10 % error of the LOPAP instrument. The average daytime diurnal cycle of the measured and modelled HONO, along with the contribution of the different sources in the model, is shown in Fig. 5. From just after sunrise (08:00 UTC), the contribution to HONO of the reaction between OH and NO decreases quickly due to the increasing $j(HONO)$ and decreasing NO levels throughout the morning. The largest contribution throughout the day comes from the photolysis of adsorbed HNO_3, contributing around 50 % of the HONO source at midday. There are small contributions during the day and from heterogeneous conversion of NO_2 (on both aerosol and ground surfaces) and the photolysis of ortho-nitrophenol. Examining the total HONO predicted by the model compared to the measurement shows a significant underestimation of the modelled HONO compared to the measurement. They do both follow a similar diurnal cycle, with a decrease in HONO until around 16:00 UTC, followed by an increase into the evening; however, the modelled HONO is up to a factor of around 2 lower than the measurement throughout the day. Subtracting the modelled from the
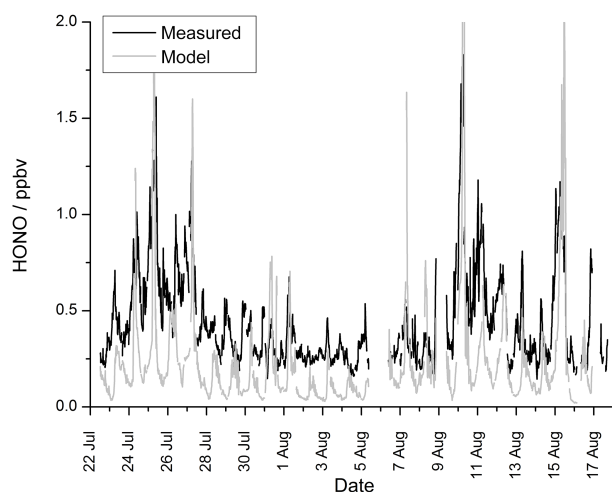
Figure 4. Time series of measured (black) and model calculated (grey) HONO during the IOP. The model was based on the Master Chemical Mechanism (MCM v3.2); see text for details.

Figure 5. Average daytime diurnal profile of the modelled HONO from different sources shown as a compound area plot, as described in Sect. 3.3 of the text. Also plotted (black trace) is the measured HONO.

Figure 6. Average daytime diurnal profile of the "missing" HONO production rate (in $ppb\,h^{-1}$), defined as the rate of HONO production required to reproduce the measurements in the model. The black trace shows average of all data, the red trace shows the average of data from easterly conditions, and the blue trace shows the average of data from westerly conditions.

measured HONO gives us a quantity that can be described as "missing" HONO source, and average diurnal daytime profile of this is plotted in Fig. 6. The amount of the missing HONO source begins to increase at 08:00 UTC and reaches a maximum at 12:00 UTC of $\sim 2.8\,ppbV\,h^{-1}$, exhibiting a similar diurnal trend to that of the HONO / NO$_x$ ratio (see Fig. 2). It then starts to decrease throughout the afternoon and into the evening. Further analysis can be carried out by examining the diurnal profiles in the easterly and westerly flow conditions described earlier. Both conditions show broadly the same diurnal profile; however, the daytime peak in missing HONO is greater in the more polluted easterly flow (up to 0.6 ppbV). This suggests that any missing source of HONO is related in some way to the pollution loading, most likely the amount of NO$_2$. This will be discussed further in later sections.

It is clear from these data that neither a photostationary state calculation nor a more complete photochemical model containing currently known and postulated sources of HONO (that are relevant for this environment) can reproduce the daytime levels measured in London during this study. This is potentially significant, as HONO can be a large source of free radicals in such an urban environment, and any missing source in models can lead to an underestimation of the oxidising capacity of the atmosphere and hence its ability to produce O$_3$. Therefore it is worth considering where the "missing" HONO may come from and the importance of any extra source to the atmospheric oxidation capacity.
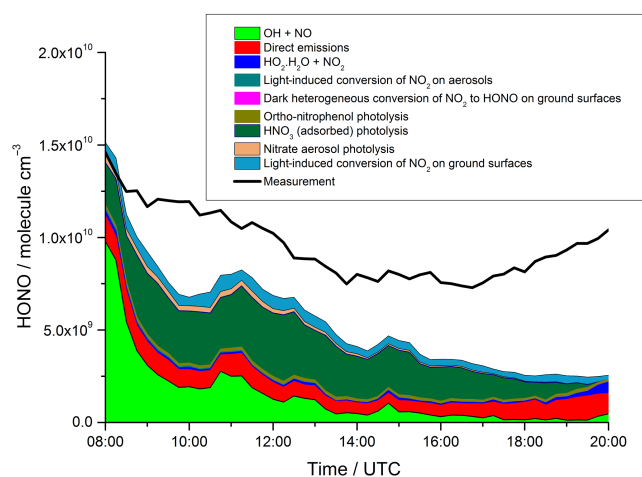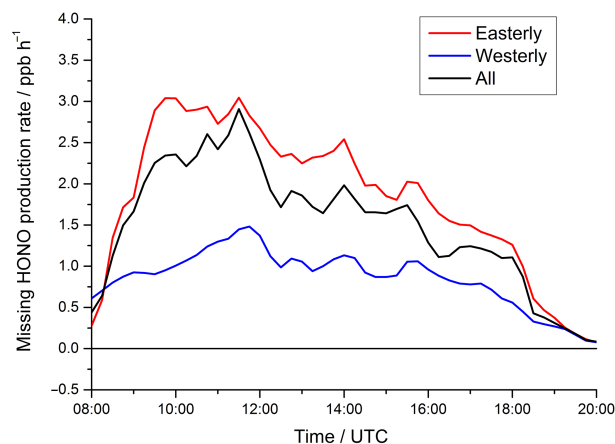
4 Discussion

4.1 Instrument interference

It is first worth considering the effect of possible instrument interferences on the HONO measurements made in this study. As described earlier, the LOPAP technique is not direct; rather it measures HONO by conversion to a coloured azo dye which is then detected by absorption spectroscopy. However, it has been postulated that HO$_2$NO$_2$ could interfere with the conversion reaction, leading to erroneous HONO measurements. A recent study by Legrand et al. (2014), using an identical instrument to the one described here and inves-

tigating apparently high measurements of HONO in Antarctica, showed in laboratory experiments that the instrument does have an interference with HO_2NO_2. Their work indicated that up to 15 % of HO_2NO_2 was converted to the azo dye in the instrument and detected as HONO. For this study, 2 ppbv of HO_2NO_2 would explain the difference between measured and modelled HONO; however, this seems unrealistic in an urban environment in summer (Dentener et al., 2002). In fact, the box model used here shows HO_2NO_2 levels to only be between 2 and 10 pptv, and therefore we feel that this instrument interference can be discounted here. For submicrometer particles we exclude any interferences by particle nitrite, since their sampling efficiency is < 2 % in the very short stripping coil (4 coil sampler). Even if that increased to values of 10 % for larger coarse particles, such interference would be almost perfectly corrected for by the two channel approach. For much larger fog particles (which actually were not present during the campaign during daytime) interferences would be only expected in the case of high fog pH vales of > 5. For lower pH, expected for the urban conditions in London, the effective solubility of HONO (HONO + nitrite) would be too low to significantly influence the HONO data, even for high uptake efficiency of fog particles. Accordingly, we do not consider particle interferences as an important issue. Finally, the LOPAP was successfully intercompared to the spectroscopic DOAS technique under urban background conditions similar to the present study (Kleffmann et al., 2006).

4.2 Missing HONO source

The ClearfLo IOP campaign involved a wide range of measurements, thus enabling the relationship between the apparent missing HONO and various other species to be investigated. Initially, daytime diurnal average profiles were plotted for NO_2 and the product $NO_2 \times j(NO_2)$, along with the extra rate of production of HONO required for the model to reproduce the measurements (termed "missing HONO source" – Fig. 7). The plots show that, whilst there is little correlation between the NO_2 on its own with the missing HONO, there appears to be a reasonable correlation with the product of NO_2 and $j(NO_2)$, hence pointing towards a photolytic source.

To further investigate any potential correlation, the full data series of the missing HONO source and different input data are normalized to 1 and correlated against each other. The normalized missing HONO source data are then correlated with the normalized products of all possible combinations of the input data. The data sets are then filtered to determine whether inclusion of an extra data set has led to a genuine increase in the correlation coefficient. For inclusion in the filtered output, the correlation coefficient for the product must be greater than the correlation coefficient for each of the individual components in the product. Additionally, inclusion of an additional data set in a product must
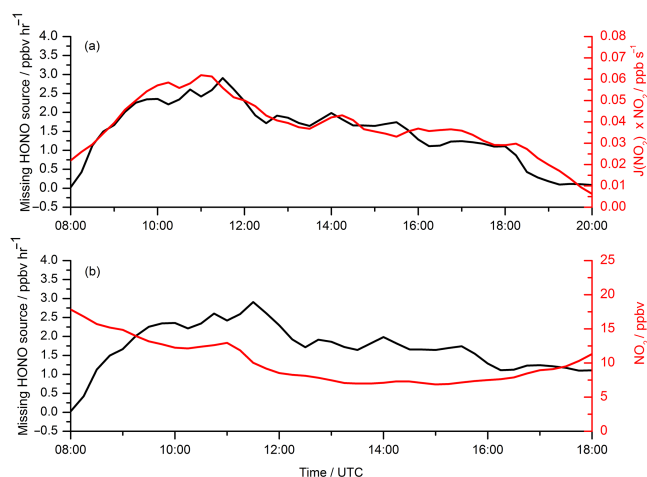

Figure 7. Average diurnal profiles of the missing HONO source (black traces) plotted with (as red traces) **(a)** $NO_2 \times j(NO_2)$ and **(b)** NO_2.

lead to an increase in the correlation coefficient for the new product when compared to the correlation coefficient without that new data set. Data sets included are $j(NO_2)$ (used as a proxy for radiation), water vapour, NO, NO_2, temperature, adsorbed HNO_3 (HNO_3ads.), OH, HO_2, RO_2, OH reactivity ($k(OH)$), nitrate aerosol (NO_3^- aero.), ammonium aerosol (NH_4^+ aero.), and aerosol SA. We use $k(OH)$ as a proxy for organic substances as it has been shown by Whalley et al. (2016), that $k(OH)$ is largely controlled by VOCs during the measurement period (typically 80 % during daytime). The correlation plots are shown in the Supplement (Fig. S1), with the correlation coefficients of the different combinations presented in Table 1. The data show that several product combinations are significantly higher than those of the individual components. For instance, the correlation coefficient with NO_2 alone is virtually 0, whereas for the product of $j(NO_2) \times NO_2$ the r^2 is 0.696, for $j(NO_2) \times k(OH)$ it is 0.678, and for $NO_2 \times k(OH) \times j(NO_2)$ the r^2 is 0.659. Thus, if gaseous VOCs (represented here by $k(OH)$) are precursors for VOCs adsorbed onto surfaces, then this is an indication that the photosensitized reaction of NO_2 on surfaces containing organics as a source of HONO may currently be underestimated in the model. We also see high correlation coefficients with $j(NO_2) \times T$ (0.628), but this can be explained by radiation and temperature following a similar diurnal pattern, albeit with a slight (1–2 h) time lag. The product of $j(NO_2)$ and ammonium aerosol (NH_4^+) is 0.583, suggesting this may play a role in the missing HONO, although any possible mechanisms for this are unclear.

In order to investigate the day-to-day variation in the potential HONO source, correlation plots were made of the daytime average (08:00–20:00 UTC) missing HONO source against NO_2 and the product of $j(NO_2)$ with NO_2, $k(OH)$ and $NO_2 \times k(OH)$ (Fig. 8). These show that there is some

Table 1. Correlation coefficients (r^2) for plots between various species measured during ClearfLo (and their products), using $j(NO_2)$ as a proxy for radiation, and the missing HONO source from the model (using the model with all additional sources). The species used were chosen using the method described in the text. See Fig. S1 in the Supplement for plots.

Species	r^2 for correlation vs. missing HONO
$j(NO_2)$	0.5394
H_2O	0.0004
NO	0.0270
NO_2	0.0001
Temp	0.3557
HNO_3ads.	0.0966
OH	0.2745
HO_2	0.1925
RO_2	0.2763
$k(OH)$	0.0001
NO_3^- aero.	0.0006
NH_4^+ aero.	0.0007
Aerosol surface area	0.0001
$j(NO_2) \times H_2O$	0.5981
$j(NO_2) \times NO_2$	0.6960
$j(NO_2) \times T$	0.6276
$j(NO_2) \times k(OH)$	0.6781
$j(NO_2) \times NH_4^+$	0.5829
$j(NO_2) \times HNO_3$ads.	0.4356
$H_2O \times HNO_3$ads.	0.1044
$H_2O \times OH$	0.3378
$H_2O \times RO_2$	0.2899
$H_2O \times NO_3^-$ aero.	0.0006
$NO \times HNO_3$	0.1276
$NO \times OH$	0.2791
$NO \times HO_2$	0.2580
$NO_2 \times OH$	0.3867
Temp $\times$ OH	0.3952
$OH \times k(OH)$	0.3497
$OH \times NH_4^+$ aero.	0.3888
$HO_2 \times k(OH)$	0.1941
$RO_2 \times k(OH)$	0.2819
$j(NO_2) \times NO_2 \times T$	0.7262
$j(NO_2) \times T \times k(OH)$	0.7069
$j(NO_2) \times NO_2 \times k(OH)$	0.6594
$NO \times HNO_3$ads. $\times$ OH	0.4085
$NO \times HNO_3$ads. $\times HO_2$	0.2916
$NO \times HNO_3$ads. $\times RO_2$	0.3198
$j(NO_2) \times H_2O \times T \times k(OH)$	0.7280

correlation for all species, with the products of the species with $j(NO_2)$ ($r^2 = 0.64$, 0.55 and 0.71 for NO_2, $k(OH)$ and $NO_2 \times k(OH)$ respectively) being significantly higher than with NO_2 alone ($r^2 = 0.33$).

Based on the correlational analysis we propose here an enhancement in the photosensitized conversion of NO_2 on organic substrates to explain the missing HONO source. In contrast, other recently proposed HONO sources will have a minor contribution. Aqueous solutions in which HONO yields from nitrate photolysis may be enhanced by organics (Scharko et al., 2014) will not be important for the urban conditions investigated in this study as there are no aqueous surfaces in the surrounding area. Recently, in the study of Rutter et al. (2014), a gas phase reduction of HNO_3 by VOCs to HONO was proposed. However, since the conditions of that laboratory study were not atmospherically relevant (reaction in the presence of ca. 200 ppb of a high molecular weight motor oil), we have not considered this source for this analysis. In addition, this is a dark reaction, while we have mainly considered the more important daytime HONO chemistry in the present manuscript. In the study of Ziemba et al. (2010) a conversion of HNO_3 on organic aerosols was proposed based on field observations. However, HONO formation was only observed in the dark, which again is out of the scope of this study. In addition the very low correlation coefficient of the missing HONO source with aerosol nitrate does not support this mechanism. Formation of HONO by soil sources (Oswald et al., 2013, 2015) is also expected to be of minor importance for London due to low soil surface coverage.

Although direct emissions were already considered in the model, we carried out a sensitivity analysis into the direct emission of HONO to study potential errors within our model. We found that increasing direct emissions by a factor of 2 (even though we think our estimate is already an upper limit) only results in a 4 % increase in the modelled HONO. Hence we do not believe direct emissions to be the source of the missing HONO. We have also run a sensitivity analysis on the heterogeneous photosensitized conversion of NO_2 on ground surfaces by increasing the conversion rate by up to a factor of 10 to assess the impact of enhanced reactive uptake of NO_2 on other surfaces, for example urban grime. We find that a reactive conversion rate of $\sim 6 \times 10^{-5}$ s^{-1} (but which varies as a function of $j(NO_2)$) closes the daytime HONO budget at all times (apart from the late afternoon). This is shown in Fig. 9, demonstrating that with an increased conversion rate, the heterogeneous photosensitized conversion of NO_2 on ground surfaces becomes the largest HONO source throughout the day. Based on this sensitivity study and on the high correlation of the missing HONO source with the products $j(NO_2) \times NO_2$ and $j(NO_2) \times NO_2 \times k(OH)$, enhanced photosensitized conversion of NO_2 on organic surfaces is proposed here as a major HONO source in London. However, the exact identification of the organics adsorbed on the urban surfaces (humic acids, organic grime, etc.) is out of the scope of the present study. In Sörgel et al. (2011b), it was shown that the results presented by Stemmler et al. (2007) on an artificial humic acid are not able to describe their field observation. The heterogeneous NO_2 uptake kinetics and HONO yields of real urban organic substrates are not known and maybe different compared to the artificial surfaces studied in the laboratory. Detailed laboratory studies
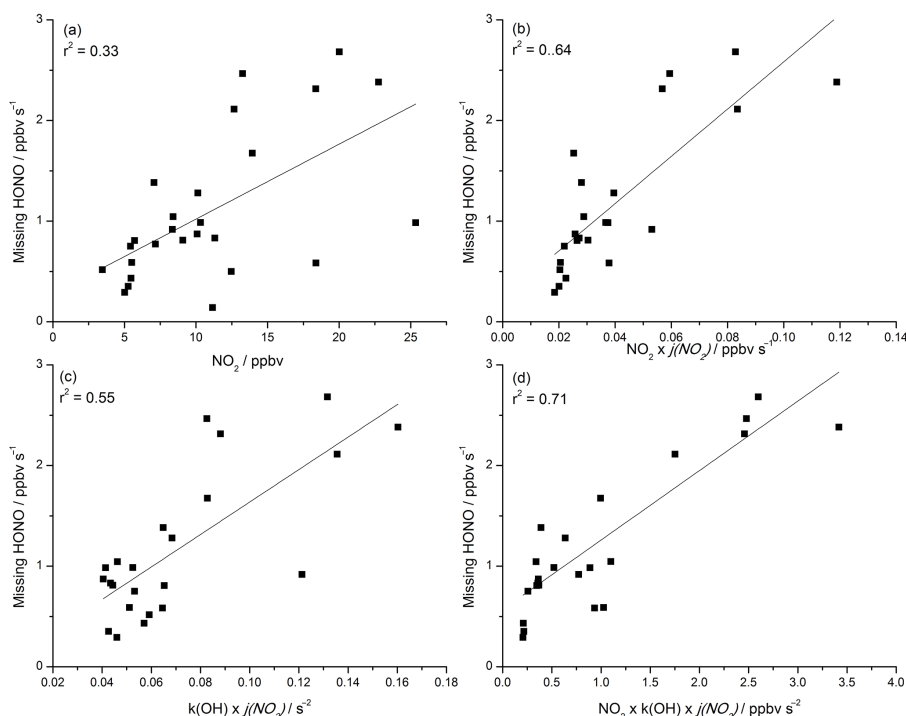
Figure 8. Daytime averaged (08:00–19:00 UTC) missing HONO source plotted against **(a)** NO_2, **(b)** $NO_2 \times j(NO_2)$, **(c)** $k(OH) \times j(NO_2)$, and **(d)** $NO_2 \times k(OH) \times j(NO_2)$.
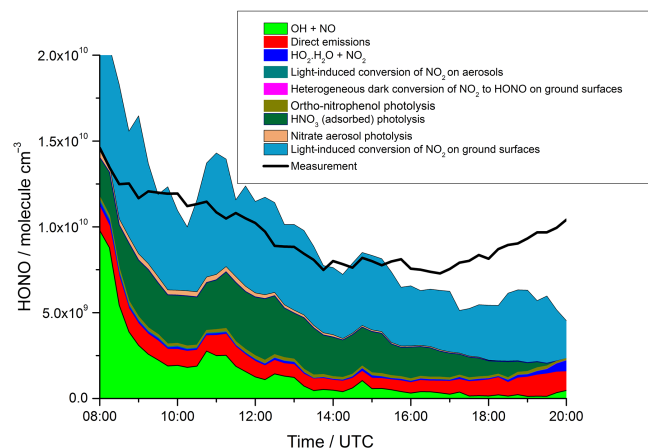

Figure 9. Average daytime diurnal profile of the modelled HONO from different sources shown as a compound area plot, as described in Sect. 3.3 of the text, showing the result of increasing the reactive uptake coefficient of the light enhanced conversion of NO_2 on ground surfaces (see text for details). Also plotted (black trace) is the measured HONO.

on real surfaces collected from the surrounding of the field site in London would be necessary, which is again out of the scope of this study.

It should also be pointed out that our model only represents the situation at the measurement height of HONO and

the supporting species (5 m) and is not used to attempt to describe the entire BL. Numerous measurements demonstrate that near-surface vertical structure in HONO can be significant at night and during the day (Stutz et al., 2002; Kleffmann et al., 2003; Kleffmann, 2007; Zhang et al., 2009; Villena et al., 2011; Wong et al., 2012; Young et al., 2012; Oswald et al., 2015) and that a model using a near-surface source distributed throughout the BL produces results inconsistent with observations (Vandenboer et al., 2013; Wong et al., 2013; Kim et al., 2014; Sörgel et al., 2015). Thus, some of the discrepancy between the model and measurements, particularly in the early morning when thermal inversions can persist, could be ascribed to biases from vertical stratification in HONO. It is, however, clear that at the present urban background site close to central London and within 5 m of the surface, a significant missing source of HONO is active when compared to the output of a box model containing most known sources. We suggest from our analysis of the supporting data that processes responsible for the unknown source of HONO in this particular study are at least partially connected with light, NO_2, and organic matter (represented by $k(OH)$), in agreement with the source described in Stemmler et al. (2006, 2007).

4.3 HONO contribution to atmospheric oxidation

HONO is known to be an important initiation source of OH radicals (Ren et al., 2003, 2006; Dusanter et al., 2009;
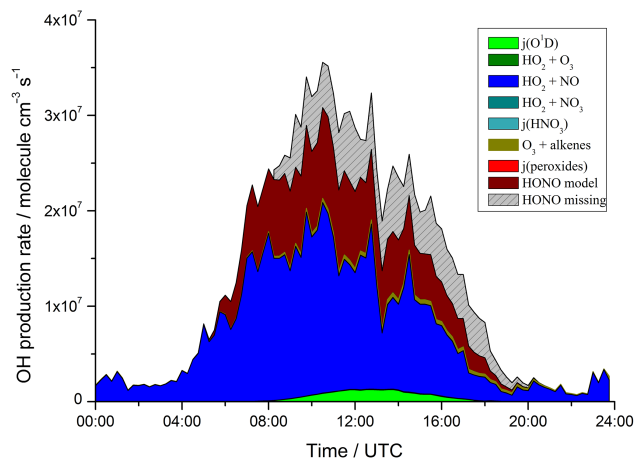
Figure 10. Average diurnal profile of gross OH production rates from different initiation and propagation sources calculated by the model.

Figure 11. Average diurnal profile of OH showing measured (black), modelled unconstrained to HONO with only $NO + OH$ as a HONO sources (green), modelled unconstrained to HONO including additional HONO sources (blue – see text for details), and model constrained to measured HONO (red).

Elshorbany et al., 2009; Hofzumahaus et al., 2009; Villena et al., 2011; Michoud et al., 2012, 2014), so any extra source that is not well understood or defined in models could have a potentially important impact on atmospheric oxidation capacity and hence O_3 and SOA production. The model described above was used to produce a rate of production analysis (ROPA) for OH radicals during the measurements campaign, with a view to assessing the importance of HONO and in particular the missing HONO source. It should again be pointed out here that any conclusions drawn from this analysis are only valid for this particular measurement site (i.e. close to the surface). The model is only being used to understand OH production at the HONO measurement height even though the chemistry is taking place in a dynamic BL. For the analysis of the vertical structure of the HONO contribution to the OH initiation, our measurement data are not sufficient and further gradient studies would be necessary. We also do not include the enhanced reactive conversion of NO_2 on other surfaces or increased direct emissions described in the sensitivity analysis in this investigation.

For this analysis, the ROPA output was plotted for all OH radical sources and the diurnal average for these is shown in Fig. 10. Initially ignoring the missing HONO source, it can be seen that in the early morning shortly after sunrise, HONO is a significant OH source (30–40 % of the total, second only to the propagation source of $NO + HO_2$). This is due to the build-up of HONO concentrations overnight, followed by its rapid photolysis after sunrise. Then, approaching solar noon, whilst the absolute production rate from HONO photolysis remains relatively constant, the dominant OH source becomes the $HO_2 + NO$ reaction. At solar noon, HONO unconstrained in the model accounts for around 40 % of the total OH radical sources and 57 % of the HO_x initiation sources. During the late afternoon and evening approaching sunset, OH from HONO photolysis again becomes comparable to
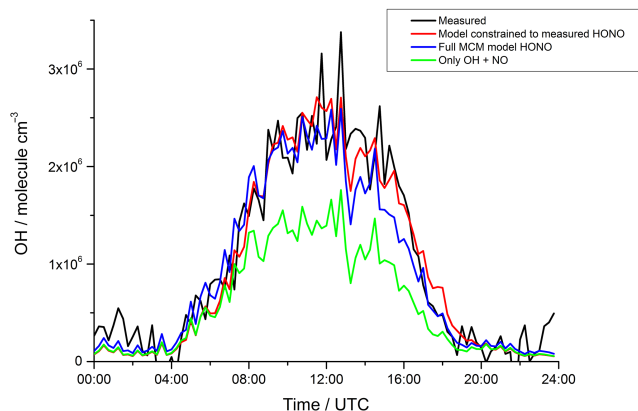
$HO_2 + NO$. The photolysis of O_3 is only a minor component of the total OH radical sources throughout the day, peaking at around 10 % in early afternoon. The same holds for the ozonolysis of alkenes which is caused, at least in part, by the low levels of measured alkenes. With the model constrained to the measured HONO, it was possible to add on the effect of the missing HONO source to OH radical production rate to the diurnal profile. It can clearly be seen that the OH production rate is significantly increased during the daytime, especially during the afternoon when constraining the model to measured HONO, where the OH production rate increases by around 20 %. This result shows that, even when all currently known sources of HONO are added to a box model, missing HONO sources are still crucial to HO_x radical production at the surface, which is directly relevant to atmospheric oxidation capacity and O_3 formation.

This importance is also shown when the model is used to calculate OH concentrations, as shown in Fig. 11. If the model is run with PSS-calculated HONO (i.e. only $OH + NO$ as a source), there is a significant underprediction of OH levels ($\sim 40\%$ during daytime). When the known or postulated HONO sources are included in the model, the predicted OH is increased by a factor of 1.4–1.6 during the day. However, during the afternoon, predicted OH is still 20–30 % lower than modelled, suggesting a missing OH source. It is only when the model is constrained to measured HONO does the agreement between measured and modelled OH become good ($< 5\%$ discrepancy at midday and during most of the afternoon) and within the experimental error of the measurements ($\sim 15\%$). This clearly demonstrates the need for models to include accurate HONO data (either from measurements or a model containing all HONO sources and sinks) and thus the need for further investigation on the missing HONO source.

5 Summary and conclusions

In this study a month-long time series of HONO levels at an urban background site in London was measured, with average mixing ratios showing a peak in the early morning of ~ 0.6 ppbV and a minimum during early afternoon of ~ 0.18 ppbV. Analysis of the HONO / NO_x ratio showed a significant secondary peak during daytime, suggesting additional sources of HONO other than the reaction between NO and OH. The presence of a large range of other atmospheric gas and aerosol measurements (including OH and HO_2 radicals) allowed a detailed study of known and postulated production routes of HONO to be undertaken, using both a simple PSS analysis and a box model based on the MCMv3.2. The calculated HONO shows a daytime underestimation of ~ 0.2 ppbV on average, even when recently suggested sources such as the reaction of $HO_2 \times H_2O$ with NO_2 to produce HONO, photolysis of adsorbed HNO_3, photoenhanced conversion of NO_2 on ground and aerosol surfaces, and direct traffic emissions are included, again suggesting a significant missing HONO source. Correlation plots of the missing HONO production rate against various other species measured at the site show a reasonable correlation with the product of $j(NO_2)$ with NO_2 and $k(OH)$, suggesting that the proposed photosensitized heterogeneous conversion of NO_2 to HONO on organic substrates as observed in laboratory studies may be enhanced under these urban conditions.

The effect of the missing source of HONO on the oxidising capacity of the urban background atmosphere has been investigated using radical rate of production analyses. These show that OH radical production during the day increases by over 20 % if measured HONO is used in the model as compared to allowing the model to run unconstrained to HONO, even with known and postulated HONO sources included. In addition, modelled OH only reproduces the measurement when HONO was constrained in the model. Whilst our results are only valid at the surface due to the likely HONO gradients, it is still an important result and demonstrates the need of a full understanding of the HONO production processes in an urban area such as London in, for example, air quality prediction models. The results presented here provide further evidence that unknown sources of HONO are present in the urban environment, and they are probably a function of NO_x and sunlight. It is not possible to conclude exactly the origin of the source from this work, hence further field measurements and, probably more crucially, laboratory studies are needed to investigate these important processes further.

The Supplement related to this article is available online at doi:10.5194/acp-16-2747-2016-supplement.

References

Acker, K., Möller, D., Wieprecht, W., Meixner, F. X., Bohn, B., Gilge, S., Plass-Dülmer, C., and Berresheim, H.: Strong daytime production of OH from HNO_2 at a rural mountain site, Geophys. Res. Lett., 33, L02809, doi:10.1029/2005gl024643, 2006.

Alicke, B., Platt, U., and Stutz, J.: Impact of nitrous acid photolysis on the total hydroxyl radical budget during the Limitation of Oxidant Production/Pianura Padana Produzione di Ozono study in Milan, J. Geophys. Res., 107, 8196, doi:10.1029/2000jd000075, 2002.

Arens, F., Gutzwiller, L., Baltensperger, U., Gäggeler, H. W., and Ammann, M.: Heterogeneous Reaction of NO_2 on Diesel Soot Particles, Environ. Sci. Technol., 35, 2191–2199, 2001.

Atkinson, R., Baulch, D. L., Cox, R. A., Crowley, J. N., Hampson, R. F., Hynes, R. G., Jenkin, M. E., Rossi, M. J., and Troe, J.: Evaluated kinetic and photochemical data for atmospheric chemistry: Volume I – gas phase reactions of O_x, HO_x, NO_x and SO_x species, Atmos. Chem. Phys., 4, 1461–1738, doi:10.5194/acp-4-1461-2004, 2004.

Barlow, J. F., Dunbar, T. M., Nemitz, E. G., Wood, C. R., Gallagher, M. W., Davies, F., O'Connor, E., and Harrison, R. M.: Boundary layer dynamics over London, UK, as observed using Doppler lidar during REPARTEE-II, Atmos. Chem. Phys., 11, 2111–2125, doi:10.5194/acp-11-2111-2011, 2011.

Barlow, J. F., Halios, C. H., Lane, S. E., and Wood, C. R.: Observations of urban boundary layer structure during a strong urban heat island event, Environ. Fluid Mech., 15, 373–398, doi:10.1007/s10652-014-9335-6, 2015.

Bejan, I., Abd El Aal, Y., Barnes, I., Benter, T., Bohn, B., Wiesen, P., and Kleffmann, J.: The photolysis of ortho-nitrophenols: a new gas phase source of HONO, Phys. Chem. Chem. Phys., 8, 2028–2035, doi:10.1039/b516590c, 2006.

Bigi, A. and Harrison, R. M.: Analysis of the air pollution climate at a central urban background site, Atmos. Environ., 44, 2004–2012, doi:10.1016/j.atmosenv.2010.02.028, 2010.

Bohnenstengel, S. I., Belcher, S. E., Aiken, A., Allan, J. D., Allen, G., Bacak, A., Bannan, T. J., Barlow, J. F., Beddows, D. C. S., Bloss, W. J., Booth, A. M., Chemel, C., Coceal, O., Di Marco, C. F., Dubey, M. K., Faloon, K. H., Fleming, Z. L., Furger, M., Gietl, J. K., Graves, R. R., Green, D. C., Grimmond, C. S. B., Halios, C. H., Hamilton, J. F., Harrison, R. M., Heal, M. R., Heard, D. E., Helfter, C., Herndon, S. C., Holmes, R. E., Hopkins, J. R., Jones, A. M., Kelly, F. J., Kotthaus, S., Langford, B., Lee, J. D., Leigh, R. J., Lewis, A. C., Lidster, R. T., Lopez-Hilfiker, F. D., McQuaid, J. B., Mohr, C., Monks, P. S., Nemitz, E., Ng, N. L., Percival, C. J., Prévôt, A. S. H., Ricketts, H. M.

A., Sokhi, R., Stone, D., Thornton, J. A., Tremper, A. H., Valach, A. C., Visser, S., Whalley, L. K., Williams, L. R., Xu, L., Young, D. E., and Zotter, P.: Meteorology, air quality, and health in London: The ClearfLo project, B. Am. Meteorol. Soc., 96, 779–804, doi:10.1175/BAMS-D-12-00245.1, 2014.

Cappa, C. D., Onasch, T. B., Massoli, P., Worsnop, D. R., Bates, T. S., Cross, E. S., Davidovits, P., Hakala, J., Hayden, K. L., Jobson, B. T., Kolesar, K. R., Lack, D. A., Lerner, B. M., Li, S.-M., Mellon, D., Nuaaman, I., Olfert, J. S., Petäjä, T., Quinn, P. K., Song, C., Subramanian, R., Williams, E. J., and Zaveri, R. A.: Radiative Absorption Enhancements Due to the Mixing State of Atmospheric Black Carbon, Science, 337, 1078–1081, doi:10.1126/science.1223447, 2012.

Dentener, F., Williams, J., and Metzger, S.: Aqueous phase reaction of HNO_4: The impact on tropospheric chemistry, J. Atmos. Chem., 41, 109–134, doi:10.1023/a:1014233910126, 2002.

Dransfield, T. J., Donahue, N. M., and Anderson, J. G.: High-Pressure Flow Reactor Product Study of the Reactions of $HO_x + NO_2$: The Role of Vibrationally Excited Intermediates†, J. Phys. Chem. A, 105, 1507–1514, doi:10.1021/jp002391+, 2001.

Drummond, J. W., Volz, A., and Ehhalt, D. H.: An Optimized Chemiluminescence Detector for Tropospheric NO Measurements, J. Atmos. Chem., 2, 287–306, doi:10.1007/bf00051078, 1985.

Dusanter, S., Vimal, D., Stevens, P. S., Volkamer, R., Molina, L. T., Baker, A., Meinardi, S., Blake, D., Sheehy, P., Merten, A., Zhang, R., Zheng, J., Fortner, E. C., Junkermann, W., Dubey, M., Rahn, T., Eichinger, B., Lewandowski, P., Prueger, J., and Holder, H.: Measurements of OH and HO_2 concentrations during the MCMA-2006 field campaign – Part 2: Model comparison and radical budget, Atmos. Chem. Phys., 9, 6655–6675, doi:10.5194/acp-9-6655-2009, 2009.

Edwards, G. D. and Monks, P. S.: Performance of a single-monochromator diode array spectroradiometer for the determination of actinic flux and atmospheric photolysis frequencies, J. Geophys. Res., 108, 8546, doi:10.1029/2002JD002844, 2003.

Elshorbany, Y. F., Kurtenbach, R., Wiesen, P., Lissi, E., Rubio, M., Villena, G., Gramsch, E., Rickard, A. R., Pilling, M. J., and Kleffmann, J.: Oxidation capacity of the city air of Santiago, Chile, Atmos. Chem. Phys., 9, 2257–2273, doi:10.5194/acp-9-2257-2009, 2009.

Forster, G. L., Sturges, W. T., Fleming, Z. L., Bandy, B. J., and Emeis, S.: A year of H_2 measurements at Weybourne Atmospheric Observatory, UK, 2012, Tellus B, 64, 17771, doi:10.3402/tellusb.v64i0.17771, 2012.

George, C., Strekowski, R. S., Kleffmann, J., Stemmler, K., and Ammann, M.: Photoenhanced uptake of gaseous NO_2 on solid organic compounds: a photochemical source of HONO?, Faraday Discuss., 130, 195–210, doi:10.1039/b417888m, 2005.

Harrison, R. M. and Kitto, A.-M. N.: Evidence for a Surface Source of Atmospheric Nitrous Acid, Atmos. Environ., 28, 1089–1094, 1994.

Heard, D. E. and Pilling, M. J.: Measurement of OH and HO_2 in the troposphere, Chem. Rev., 103, 5163–5198, 2003.

Heland, J., Kleffmann, J., Kurtenbach, R., and Wiesen, P.: A New Instrument To Measure Gaseous Nitrous Acid (HONO) in the Atmosphere, Environ. Sci. Technol., 35, 3207–3212, doi:10.1021/es000303t, 2001.

Hofzumahaus, A., Rohrer, F., Lu, K. D., Bohn, B., Brauers, T., Chang, C. C., Fuchs, H., Holland, F., Kita, K., Kondo, Y., Li, X., Lou, S., Shao, M., Zeng, L., Wahner, A., and Zhang, Y.: Amplified Trace Gas Removal in the Troposphere, Science, 324, 1702–1704, 2009.

Hopkins, J. R., Lewis, A. C., and Read, K. A.: A two-column method for long-term monitoring of non-methane hydrocarbons (NMHCs) and oxygenated volatile organic compounds (o-VOCs), J. Environ. Monit., 5, 8–13, 2003.

Jenkin, M. E., Wyche, K. P., Evans, C. J., Carr, T., Monks, P. S., Alfarra, M. R., Barley, M. H., McFiggans, G. B., Young, J. C., and Rickard, A. R.: Development and chamber evaluation of the MCM v3.2 degradation scheme for β-caryophyllene, Atmos. Chem. Phys., 12, 5275–5308, doi:10.5194/acp-12-5275-2012, 2012.

Joyce, P. L., von Glasow, R., and Simpson, W. R.: The fate of NO_x emissions due to nocturnal oxidation at high latitudes: 1-D simulations and sensitivity experiments, Atmos. Chem. Phys., 14, 7601–7616, doi:10.5194/acp-14-7601-2014, 2014.

Kim, S., Vandenboer, T. C., Young, C. J., Riedel, T. P., Thornton, J. A., Swarthout, B., Sive, B., Lerner, B., Gilman, J. B., Warneke, C., Roberts, J. M., Guenther, A. B., Wagner, N. L., Dubé, W. P., Williams, E., and Brown, S. S.: The primary and recycling sources of OH during the NACHT-2011 campaign: HONO as an important OH primary source in the wintertime, J. Geophys. Res., 119, 6886–6896, doi:10.1002/2013JD020225, 2014.

Kleffmann, J.: Daytime sources of nitrous acid (HONO) in the atmospheric boundary layer, Chem. Phys. Chem., 8, 1137–1144, doi:10.1002/cphc.200700016, 2007.

Kleffmann, J., Becker, K. H., Lackhoff, M., and Wiesen, P.: Heterogeneous Conversion of NO_2 on Carbonaceous Surfaces, Phys. Chem. Chem. Phys., 1, 5443–5450, 1999.

Kleffmann, J., Kurtenbach, R., Lörzer, J., Wiesen, P., Kalthoff, N., Vogel, B., and Vogel, H.: Measured and Simulated Vertical Profiles of Nitrous Acid, Part I: Field Measurements, Atmos. Environ, 37, 2949–2955, 2003.

Kleffmann, J., Gavriloaiei, T., Hofzumahaus, A., Holland, F., Koppmann, R., Rupp, L., Schlosser, E., Siese, M., and Wahner, A.: Daytime formation of nitrous acid: A major source of OH radicals in a forest, Geophys. Res. Lett., 32, L05818, doi:10.1029/2005gl022524, 2005.

Kleffmann, J., Lörzer, J. C., Wiesen, P., Kern, C., Trick, S., Volkamer, R., Rodenas, M., and Wirtz, K.: Intercomparison of the DOAS and LOPAP techniques for the detection of nitrous acid (HONO), Atmos. Environ., 40, 3640–3652, doi:10.1016/j.atmosenv.2006.03.027, 2006.

Kraus, A. and Hofzumahaus, A.: Field measurements of atmospheric photolysis frequencies for O_3, NO_2, HCHO, CH_3CHO, H_2O_2, and HONO by UV spectroradiometry, J. Atmos. Chem., 31, 161–180, doi:10.1023/a:1005888220949, 1998.

Kurtenbach, R., Becker, K. H., Gomes, J. A. G., Kleffmann, J., Lörzer, J. C., Spittler, M., Wiesen, P., Ackermann, R., Geyer, A., and Platt, U.: Investigations of emissions and heterogeneous formation of HONO in a road traffic tunnel, Atmos. Environ., 35, 3385–3394, doi:10.1016/s1352-2310(01)00138-8, 2001.

Lee, B. H., Wood, E. C., Herndon, S. C., Lefer, B. L., Luke, W. T., Brune, W. H., Nelson, D. D., Zahniser, M. S., and Munger, J. W.: Urban measurements of atmospheric nitrous acid: A caveat on the interpretation of the HONO photo-

stationary state, J. Geophys. Res.-Atmos., 118, 12274–12281, doi:10.1002/2013JD020341, 2013.

Lee, J. D., Moller, S. J., Read, K. A., Lewis, A. C., Mendes, L., and Carpenter, L. J.: Year-round measurements of nitrogen oxides and ozone in the tropical North Atlantic marine boundary layer, J. Geophys. Res., 114, D21302, doi:10.1029/2009jd011878, 2009.

Legrand, M., Preunkert, S., Frey, M., Bartels-Rausch, Th., Kukui, A., King, M. D., Savarino, J., Kerbrat, M., and Jourdain, B.: Large mixing ratios of atmospheric nitrous acid (HONO) at Concordia (East Antarctic Plateau) in summer: a strong source from surface snow?, Atmos. Chem. Phys., 14, 9963–9976, doi:10.5194/acp-14-9963-2014, 2014.

Levy II, H.: Normal Atmosphere: Large Radical and Formaldehyde Concentrations Predicted, Science, 173, 141–143, 1971.

Li, S., Matthews, J., and Sinha, A.: Atmospheric hydroxyl radical production from electronically excited NO_2 and H_2O, Science, 319, 1657–1660, doi:10.1126/science.1151443, 2008.

Li, X., Rohrer, F., Hofzumahaus, A., Brauers, T., Häseler, R., Bohn, B., Broch, S., Fuchs, H., Gomm, S., Holland, F., Jäger, J., Kaiser, J., Keutsch, F. N., Lohse, I., Lu, K., Tillmann, R., Wegener, R., Wolfe, G. M., Mentel, T. F., Kiendler-Scharr, A., and Wahner, A.: Missing Gas-Phase Source of HONO Inferred from Zeppelin Measurements in the Troposphere, Science, 344, 292–296, doi:10.1126/science.1248999, 2014.

Lidster, R. T., Hamilton, J. F., Lee, J. D., Lewis, A. C., Hopkins, J. R., Punjabi, S., Rickard, A. R., and Young, J. C.: The impact of monoaromatic hydrocarbons on OH reactivity in the coastal UK boundary layer and free troposphere, Atmos. Chem. Phys., 14, 6677–6693, doi:10.5194/acp-14-6677-2014, 2014.

Michoud, V., Kukui, A., Camredon, M., Colomb, A., Borbon, A., Miet, K., Aumont, B., Beekmann, M., Durand-Jolibois, R., Perrier, S., Zapf, P., Siour, G., Ait-Helal, W., Locoge, N., Sauvage, S., Afif, C., Gros, V., Furger, M., Ancellet, G., and Doussin, J. F.: Radical budget analysis in a suburban European site during the MEGAPOLI summer field campaign, Atmos. Chem. Phys., 12, 11951–11974, doi:10.5194/acp-12-11951-2012, 2012.

Michoud, V., Colomb, A., Borbon, A., Miet, K., Beekmann, M., Camredon, M., Aumont, B., Perrier, S., Zapf, P., Siour, G., Ait-Helal, W., Afif, C., Kukui, A., Furger, M., Dupont, J. C., Haeffelin, M., and Doussin, J. F.: Study of the unknown HONO daytime source at a European suburban site during the MEGAPOLI summer and winter field campaigns, Atmos. Chem. Phys., 14, 2805–2822, doi:10.5194/acp-14-2805-2014, 2014.

Monge, M. E., D'Anna, B., Mazri, L., Giroir-Fendler, A., Ammann, M., Donaldson, D. J., and George, C.: Light changes the atmospheric reactivity of soot, P. Natl. Acad. Sci. USA, 107, 6605–6609, doi:10.1073/pnas.0908341107, 2010.

Oswald R., Behrendt, T., Ermel, M., Wu, D., Su, H., Cheng, Y., Breuninger, C., Moravek, A., Mougin, E., Delon, C., Loubet, B., Pommerening-Röser, A., Sörgel, M., Pöschl, U., Hoffmann, T., Andreae, M. O., Meixner, F. X., and Trebs, I.: HONO Emissions from Soil Bacteria as a Major Source of Atmospheric Reactive Nitrogen, Science, 341, 1233–1235, 2013.

Oswald, R., Ermel, M., Hens, K., Novelli, A., Ouwersloot, H. G., Paasonen, P., Petäjä, T., Sipilä, M., Keronen, P., Bäck, J., Königstedt, R., Hosaynali Beygi, Z., Fischer, H., Bohn, B., Kubistin, D., Harder, H., Martinez, M., Williams, J., Hoffmann, T., Trebs, I., and Sörgel, M.: A comparison of HONO budgets for two measurement heights at a field station within the boreal forest in Finland, Atmos. Chem. Phys., 15, 799–813, doi:10.5194/acp-15-799-2015, 2015.

Pollack, I. B., Lerner, B. M., and Ryerson, T. B.: Evaluation of ultraviolet light-emitting diodes for detection of atmospheric NO_2 by photolysis – chemiluminescence, J. Atmos. Chem., 65, 111–125, doi:10.1007/s10874-011-9184-3, 2010.

Qin, M., Xie, P., Su, H., Gu, J., Peng, F., Li, S., Zeng, L., Liu, J., Liu, W., and Zhang, Y.: An observational study of the $HONO-NO_2$ coupling at an urban site in Guangzhou City, South China, Atmos. Environ., 43, 5731–5742, doi:10.1016/j.atmosenv.2009.08.017, 2009.

Ren, X., Brune, W. H., Oliger, A., Metcalf, A. R., Simpas, J. B., Shirley, T., Schwab, J. J., Bai, C. H., Roychowdhury, U., Li, Y. Q., Cai, C. X., Demerjian, K. L., He, Y., Zhou, X. L., Gao, H. L., and Hou, J.: OH, HO_2, and OH reactivity during the PMTACS-NY Whiteface Mountain 2002 campaign: Observations and model comparison, J. Geophys. Res., 111, D10S03, doi:10.1029/2005JD006126, 2006.

Ren, X., Sanders, J. E., Rajendran, A., Weber, R. J., Goldstein, A. H., Pusede, S. E., Browne, E. C., Min, K.-E., and Cohen, R. C.: A relaxed eddy accumulation system for measuring vertical fluxes of nitrous acid, Atmos. Meas. Tech., 4, 2093–2103, doi:10.5194/amt-4-2093-2011, 2011.

Ren, X. R., Harder, H., Martinez, M., Lesher, R. L., Oliger, A., Simpas, J. B., Brune, W. H., Schwab, J. J., Demerjian, K. L., He, Y., Zhou, X., and Gao, H.: OH and HO_2 chemistry in the urban atmosphere of New York City, Atmos. Environ., 37, 3639–3651, 2003.

Rutter, A. P., Malloy, Q. G. J., Leong, Y. J., Gutierrez, C. V., Calzada, M., Scheuer, E., Dibb, J. E., and Griffin, R. J.: The reduction of HNO_3 by volatile organic compounds emitted by motor vehicles, Atmos. Environ., 87, 200–206, doi:10.1016/j.atmosenv.2014.01.056, 2014.

Salmon, R. A., Bauguitte, S. J. B., Bloss, W., Hutterli, M. A., Jones, A. E., Read, K., and Wolff, E. W.: Measurement and interpretation of gas phase formaldehyde concentrations obtained during the CHABLIS campaign in coastal Antarctica, Atmos. Chem. Phys., 8, 4085–4093, doi:10.5194/acp-8-4085-2008, 2008.

Sander, S. P. and Peterson, M. E.: Kinetics of the Reaction $HO_2 + NO_2 + M = HO_2NO_2 + M$, J. Phys. Chem., 88, 1566–1571, doi:10.1021/j150652a025, 1984.

Scharko, N. K., Berke, A. E., and Raff, J. D.: Release of Nitrous Acid and Nitrogen Dioxide from Nitrate Photolysis in Acidic Aqueous Solutions, Environ. Sci. Technol., 48, 11991–12001, doi:10.1021/es503088x, 2014.

Sörgel, M., Trebs, I., Serafimovich, A., Moravek, A., Held, A., and Zetzsch, C.: Simultaneous HONO measurements in and above a forest canopy: influence of turbulent exchange on mixing ratio differences, Atmos. Chem. Phys., 11, 841–855, doi:10.5194/acp-11-841-2011, 2011a.

Sörgel, M., Regelin, E., Bozem, H., Diesch, J.-M., Drewnick, F., Fischer, H., Harder, H., Held, A., Hosaynali-Beygi, Z., Martinez, M., and Zetzsch, C.: Quantification of the unknown HONO daytime source and its relation to NO_2, Atmos. Chem. Phys., 11, 10433–10447, doi:10.5194/acp-11-10433-2011, 2011b.

Sörgel, M., Trebs, I., Wu, D., and Held, A.: A comparison of measured HONO uptake and release with calculated source strengths in a heterogeneous forest environment, Atmos. Chem. Phys., 15, 9237–9251, doi:10.5194/acp-15-9237-2015, 2015.

Steinbacher, M., Zellweger, C., Schwarzenbach, B., Bugmann, S., Buchmann, B., Ordonez, C., Prevot, A. S. H., and Hueglin, C.: Nitrogen oxide measurements at rural sites in Switzerland: Bias of conventional measurement techniques, J. Geophys. Res., 112, D11307, doi:10.1029/2006jd007971, 2007.

Stemmler, K., Ammann, M., Donders, C., Kleffmann, J., and George, C.: Photosensitized reduction of nitrogen dioxide on humic acid as a source of nitrous acid, Nature, 440, 195–198, doi:10.1038/nature04603, 2006.

Stemmler, K., Ndour, M., Elshorbany, Y., Kleffmann, J., D'Anna, B., George, C., Bohn, B., and Ammann, M.: Light induced conversion of nitrogen dioxide into nitrous acid on submicron humic acid aerosol, Atmos. Chem. Phys., 7, 4237–4248, doi:10.5194/acp-7-4237-2007, 2007.

Stone, D. and Rowley, D. M.: Kinetics of the Gas Phase HO_2 Self-Reaction: Effects of Temperature, Pressure, Water and Methanol Vapours, Phys. Chem. Chem. Phys., 7, 2156–2163, 2005.

Stutz, J., Alicke, B., and Neftel, A.: Nitrous acid formation in the urban atmosphere: Gradient measurements of NO_2 and HONO over grass in Milan, Italy, J. Geophys. Res., 107, 8192, doi:10.1029/2001jd000390, 2002.

Su, H., Cheng, Y. F., Cheng, P., Zhang, Y. H., Dong, S., Zeng, L. M., Wang, X., Slanina, J., Shao, M., and Wiedensohler, A.: Observation of nighttime nitrous acid (HONO) formation at a non-urban site during PRIDE-PRD2004 in China, Atmos. Environ., 42, 6219–6232, doi:10.1016/j.atmosenv.2008.04.006, 2008a.

Su, H., Cheng, Y. F., Shao, M., Gao, D. F., Yu, Z. Y., Zeng, L. M., Slanina, J., Zhang, Y. H., and Wiedensohler, A.: Nitrous acid (HONO) and its daytime sources at a rural site during the 2004 PRIDE-PRD experiment in China, J. Geophys. Res.-Atmos., 113, D14312, doi:10.1029/2007jd009060, 2008b.

Su, H., Cheng, Y., Oswald, R., Behrendt, T., Trebs, I., Meixner, F. X., Andreae, M. O., Cheng, P., Zhang, Y., and Pöschl, U.: Soil Nitrite as a Source of Atmospheric HONO and OH Radicals, Science, 333, 1616–1618, doi:10.1126/science.1207687, 2011.

Trebs, I., Lara, L. L., Zeri, L. M. M., Gatti, L. V., Artaxo, P., Dlugi, R., Slanina, J., Andreae, M. O., and Meixner, F. X.: Dry and wet deposition of inorganic nitrogen compounds to a tropical pasture site (Rondônia, Brazil), Atmos. Chem. Phys., 6, 447–469, doi:10.5194/acp-6-447-2006, 2006.

Tyndall, G. S., Orlando, J. J., and Calvert, J. G.: Upper Limit for the Rate Coefficient for the Reaction $HO_2 + NO_2 \rightarrow HONO + O_2$, Environ. Sci. Technol., 29, 202–206, doi:10.1021/es00001a026, 1995.

VandenBoer, T. C., Brown, S. S., Murphy, J. G., Keene, W. C., Young, C. J., Pszenny, A. A. P., Kim, S., Warneke, C., de Gouw, J. A., Maben, J. R., Wagner, N. L., Riedel, T. P., Thornton, J. A., Wolfe, D. E., Dubé, W. P., Öztürk, F., Brock, C. A., Grossberg, N., Lefer, B., Lerner, B., Middlebrook, A. M., and Roberts, J. M.: Understanding the role of the ground surface in HONO vertical structure: High resolution vertical profiles during NACHTT-11, J. Geophys. Res., 118, 10155–10171, doi:10.1002/jgrd.50721, 2013.

Villena, G., Kleffmann, J., Kurtenbach, R., Wiesen, P., Lissi, E., Rubio, M. A., Croxatto, G., and Rappenglück, B.: Vertical gradients of HONO, NO_x and O_3 in Santiago de Chile, Atmos. Environ., 45, 3867–3873, doi:10.1016/j.atmosenv.2011.01.073, 2011.

Villena, G., Bejan, I., Kurtenbach, R., Wiesen, P., and Kleffmann, J.: Interferences of commercial NO_2 instruments in the urban atmo-sphere and in a smog chamber, Atmos. Meas. Tech., 5, 149–159, doi:10.5194/amt-5-149-2012, 2012.

Vogel, B., Vogel, H., Kleffmann, J., and Kurtenbach, R.: Measured and simulated vertical profiles of nitrous acid – Part II. Model simulations and indications for a photolytic source, Atmos. Environ., 37, 2957–2966, doi:10.1016/S1352-2310(03)00243-7, 2003.

Whalley, L. K., Blitz, M. A., Desservettaz, M., Seakins, P. W., and Heard, D. E.: Reporting the sensitivity of laser-induced fluorescence instruments used for HO_2 detection to an interference from RO_2 radicals and introducing a novel approach that enables HO_2 and certain RO_2 types to be selectively measured, Atmos. Meas. Tech., 6, 3425–3440, doi:10.5194/amt-6-3425-2013, 2013.

Whalley, L. K., Stone, D., George, I. J., Mertes, S., van Pinxteren, D., Tilgner, A., Herrmann, H., Evans, M. J., and Heard, D. E.: The influence of clouds on radical concentrations: observations and modelling studies of HO_x during the Hill Cap Cloud Thuringia (HCCT) campaign in 2010, Atmos. Chem. Phys., 15, 3289–3301, doi:10.5194/acp-15-3289-2015, 2015.

Whalley, L. K., Stone, D., Bandy, B., Dunmore, R., Hamilton, J. F., Hopkins, J., Lee, J. D., Lewis, A. C., and Heard, D. E.: Atmospheric OH reactivity in central London: observations, model predictions and estimates of in situ ozone production, Atmos. Chem. Phys., 16, 2109–2122, doi:10.5194/acp-16-2109-2016, 2016.

Wong, K. W., Tsai, C., Lefer, B., Haman, C., Grossberg, N., Brune, W. H., Ren, X., Luke, W., and Stutz, J.: Daytime HONO vertical gradients during SHARP 2009 in Houston, TX, Atmos. Chem. Phys., 12, 635–652, doi:10.5194/acp-12-635-2012, 2012.

Wong, K. W., Tsai, C., Lefer, B., Grossberg, N., and Stutz, J.: Modeling of daytime HONO vertical gradients during SHARP 2009, Atmos. Chem. Phys., 13, 3587–3601, doi:10.5194/acp-13-3587-2013, 2013.

Ye, C., Zhou, X., Pu, D., Stutz, J., Festa, J., Spolaor, M., Cantrell, C., Mauldin, R. L., Weinheimer, A., and Haggerty, J.: Comment on "Missing Gas-phase Source of HONO Inferred from Zeppelin Measurements in the Troposphere", Science, 348, 1326–1326, doi:10.1126/science.aaa1992, 2015.

Young, C. J., Washenfelder, R. A., Roberts, J. M., Mielke, L. H., Osthoff, H. D., Tsai, C., Pikelnaya, O., Stutz, J., Veres, P. R., Cochran, A. K., Vandenboer, T. C., Flynn, J., Grossberg, N., Haman, C. L., Lefer, B., Stark, H., Graus, M., De Gouw, J., Gilman, J. B., Kuster, W. C., and Brown, S. S.: Vertically resolved measurements of nighttime radical reservoirs in Los Angeles and their contribution to the urban radical budget, Environ. Sci. Technol., 46, 10965–10973, doi:10.1021/es302206a, 2012.

Young, D. E., Allan, J. D., Williams, P. I., Green, D. C., Harrison, R. M., Yin, J., Flynn, M. J., Gallagher, M. W., and Coe, H.: Investigating a two-component model of solid fuel organic aerosol in London: processes, PM_1 contributions, and seasonality, Atmos. Chem. Phys., 15, 2429–2443, doi:10.5194/acp-15-2429-2015, 2015.

Zhang, N., Zhou, X., Shepson, P. B., Gao, H., Alaghmand, M., and Stirm, B.: Aircraft measurement of HONO vertical profiles over a forested region, Geophys. Res. Lett., 36, L15820, doi:10.1029/2009GL038999, 2009.

Zhang, N., Zhou, X., Bertman, S., Tang, D., Alaghmand, M., Shepson, P. B., and Carroll, M. A.: Measurements of ambient HONO concentrations and vertical HONO flux above a northern

Michigan forest canopy, Atmos. Chem. Phys., 12, 8285–8296, doi:10.5194/acp-12-8285-2012, 2012.

Zhou, X., Civerolo, K., Dai, H., Huang, G., Schwab, J., and Demerjian, K.: Summertime nitrous acid chemistry in the atmospheric boundary layer at a rural site in New York State, J. Geophys. Res., 107, 4590, doi:10.1029/2001jd001539, 2002.

Zhou, X., Gao, H., He, Y., Huang, G., Bertman, S. B., Civerolo, K., and Schwab, J.: Nitric acid photolysis on surfaces in low-NO_x environments: Significant atmospheric implications, Geophys. Res. Lett., 30, 2217, doi:10.1029/2003gl018620, 2003.

Zhou, X., Zhang, N., TerAvest, M., Tang, D., Hou, J., Bertman, S., Alaghmand, M., Shepson, P. B., Carroll, M. A., Griffith, S., Dusanter, S., and Stevens, P. S.: Nitric acid photolysis on forest canopy surface as a source for tropospheric nitrous acid, Nat. Geosci., 4, 440–443, doi:10.1038/NGEO1164, 2011.

Ziemba, L. D., Dibb, J. E., Griffin, R. J., Anderson, C. H., Whitlow, S. I., Lefer, B. L., Rappenglück, B., and Flynn, J.: Heterogeneous conversion of nitric acid to nitrous acid on the surface of primary organic aerosol in an urban atmosphere, Atmos. Environ., 44, 4081–4089, doi:10.1016/j.atmosenv.2008.12.024, 2010.